

Short-range Charge and Spin Superstructures in Doped Layered Co Perovskites

N. Sakiyama,¹ I. A. Zaliznyak,^{2,*} S. -H. Lee,³ Y. Mitsui,¹ and H. Yoshizawa¹

¹Neutron Science Laboratory, Institute for Solid State Physics, University of Tokyo, Tokai 319-1106, Japan

²DCMPMS, Brookhaven National Laboratory, Upton, NY 11973

³Department of Physics, University of Virginia, Charlottesville, Virginia 22904, USA

(Dated: September 15, 2021)

We have investigated cobaltite relatives of the layered perovskite cuprates and nickelates, $\text{Pr}_{2-x}\text{Ca}_x\text{CoO}_4$ ($0.39 \leq x \leq 0.73$) and $\text{La}_{2-x}\text{Sr}_x\text{CoO}_4$ ($x = 0.61$), using elastic neutron scattering. We have discovered doping-dependent incommensurate short-range ordering of charges and magnetic moments, which in cobaltites occur in the range of heavy doping, $0.5 \lesssim x \lesssim 0.75$. The charge order exists already at room temperature and shows no change on cooling. The incommensurability of its propagation vector, $\mathbf{Q}_c = (\epsilon_c, 0, l)$, roughly scales with the concentration of Co^{2+} ions, $\epsilon_c \sim (1-x)$. Magnetic order is only established at low $T \lesssim 40$ K and has twice larger periodicity, indicating a dominant antiferromagnetic correlation between the nearest Co^{2+} spins.

PACS numbers: 71.27.+a 71.28.+d 71.30.+h 71.45.Lr 72.80.Ga 75.25.+z 75.40.Cx

Physical origins of the ubiquitous doping-dependent incommensurate charge and spin ordering (CO and SO) in doped $\text{La}_{2-x}\text{Sr}_x\text{CuO}_4$ cuprates and their relevance to mechanisms of the high-temperature superconductivity have been subjects of intense research for more than a decade but still remain a mystery. Numerous experimental studies have shown, that holes in weakly doped cuprates exhibit an in-plane CO, whose propagation vector scales roughly proportionally with doping x and magnetic order, whose modulation period is twice larger [1, 2, 3]. Similar findings were reported in closely related, isostructural but insulating layered perovskite nickelates $\text{La}_{2-x}\text{Sr}_x\text{NiO}_4$ [4, 5, 6, 7, 8]. A simple picture of the simultaneous real-space static ordering of charges and spins yielding such CO and SO is provided by the charge stripe model, where doped holes segregate into lines separating stripes of antiferromagnetically ordered domains [1].

The charge stripe picture is strongly supported by theoretical analysis of the two-dimensional (2D) Hubbard model, which is believed to describe high- T_c cuprates [3, 9, 10, 11, 12]. In the 2D Hubbard model charge stripe and antiferromagnetic spin order are intimately coupled, as both are signatures of the same ordering instability of interacting itinerant charges. This model, however, discards charge immobilization effects, such as their trapping by local polarons. Doped holes in charge stripe picture are intrinsically highly mobile and decrease their energy by one-dimensional (1D) delocalization. While this assumption seems justified for moderately to highly doped cuprates, which show metallic conductivity and where an activated charge transport occurs only at low temperatures and is associated with the onset of CO in the form of "parallel stripes" aligned with Cu-O bonds [13], it is in question for lightly doped insulating cuprates and for the insulating nickelates [14, 15], where CO corresponding to the so-called "diagonal" stripes with charge lines at 45° to Cu-O bonds is observed.

In fact, cuprates are rather exceptional among Mott-Hubbard insulators (MHI), as most MHI cannot be made metallic by doping: strong polaronic self-localization of doped holes hinders metallic transport [15]. Theoretically, however, stripe-like superstructures whose period depends on the doping level are also predicted in systems with localized doped charges [16]. They are natural response of the crystal lattice to a strain associated with doping and can be explained by considering the system's elastic energy. In this picture CO is a cooperative ordering of polarons driven by lattice elastic interactions [15, 16]. So, are CO and SO scattering patterns with spin and charge incommensurabilities related by $\delta_s \sim \epsilon_c/2$ a characteristic signature of charge stripes – a 1D segregation of itinerant charges, or a ubiquitous feature of doped MHI, independent of conducting properties?

In an attempt to answer this question we have studied layered perovskite cobalt oxide series $\text{Pr}_{2-x}\text{Ca}_x\text{CoO}_4$ (PCCoO), $0.39 \leq x \leq 0.73$, and $\text{La}_{2-x}\text{Sr}_x\text{CoO}_4$ (LSCoO), $x = 0.61$, isostructural with 2D cuprates and nickelates. The undoped ($x = 0$) LSCoO parent material is a charge-transfer (CT) antiferromagnetic insulator with $T_N \approx 275$ K [17]. Magnetic Co^{2+} are in $3d^7$ ($t_{2g}^5 e_g^2$) state and, like Cu^{2+} , are Kramers ions, albeit with spin $S=3/2$. Hund's coupling in cobaltites is in close competition with the crystal field (CF), so doped holes can yield Co^{3+} ($3d^6$) in an intermediate (IS, $S=1$) or low spin (LS, $S=0$) state [18, 19, 20]. In either case the ground state in the crystal field is $S^z = 0$ singlet and is effectively non-magnetic at low T [18]. This is a fundamental consequence of Kramers time-reversal symmetry and makes comparison with cuprates particularly meaningful (Hund's rule is not at play for a single hole in $3d^9$ Cu^{2+} , while covalency and strong correlation yield a non-Hund $S = 0$ singlet $3d^8$ state for doped holes). Similar to the cuprate case, magnetic ordering temperature in LSCoO drops dramatically with doping. For $x = 0.5$ glassy SO only appears below ~ 30 K.

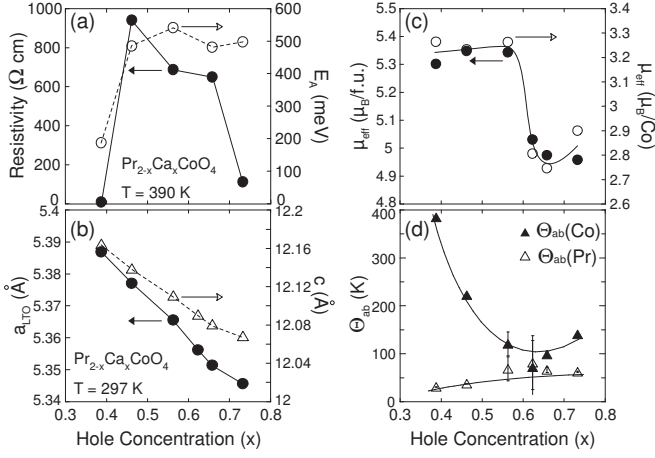


FIG. 1: Doping dependence of electrical, structural and magnetic properties of PCCoO. (a) resistivity at the highest measured temperature (closed symbols) and its activation energy (open). (b) F4/mmm ("LTO") lattice parameters refined at room temperature by powder Xray. (c) effective magnetic moment μ_{eff} per formula unit obtained by one-component Curie-Weiss analysis of the in-plane magnetic susceptibility $\chi_{ab}(T)$, $50 \text{ K} \leq T \leq 300 \text{ K}$, which includes Pr^{3+} contribution (left scale, closed symbols). Open symbols are μ_{eff} per Co ion obtained from two-component Curie-Weiss fit with fixed $\mu_{eff}^{Pr} = 3.58\mu_B$; (d) shows Weiss temperatures for Co (filled) and Pr (open) from this fit, lines are guide for the eye.

Unlike cuprates, layered LSCoO cobaltites remain insulating throughout the doping range $0 \leq x \lesssim 1$, which is in fact typical for a doped CT/MHI [20, 21]. Doped holes in cobaltites are strongly localized, so that *ab*-plane resistivity in LSCoO is in the $\sim 10 \text{ } \Omega\text{-cm}$ ($x = 1$) to $\gtrsim 10^4 \text{ } \Omega\text{-cm}$ ($x \lesssim 0.5$) range and shows polaronic activated behavior with activation energy $E_a \sim 1500 \text{ K}$ to $E_a \gtrsim 5000 \text{ K}$, respectively [20]. Short-range checkerboard charge order (CCO), which has been observed by neutron scattering in the $x = 0.5$ sample at $T \lesssim 825 \text{ K}$ [18] is thus a correlated polaron glass phase. It should be noted, that CCO can be considered a limiting case of charge stripe order with shortest possible stripe spacing, and this is how it was interpreted in the $x = 0.5$ nickelate [6, 7]. In LSCoO, however, detailed investigation of CO diffuse scattering showed no evidence for incipient 1D charge stripes [22]. In addition, polaron CO is totally independent of spins, which only order at $T \lesssim 30 \text{ K}$.

Polaronic self-localization of doped holes is similarly strong in PCCoO series. Electrical resistivity and thermal activation energy measured by PPMS in our single crystal samples are shown in Figure 1(a). Samples were grown by the floating zone method and their uniformity was verified by Scanning Electron Microscopy. The actual chemical composition x was then determined using the Inductively Coupled Plasma method. The absence of impurity phases was confirmed by powder x-ray diffraction. Samples were further characterized by measuring static magnetic susceptibility by MPMS SQUID magnetometer. Typical data is presented in the inset to Figure

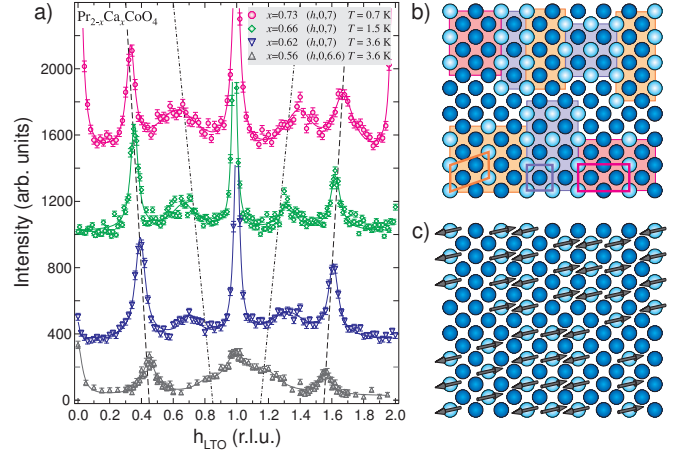


FIG. 2: (a) Elastic scans along $(h, 0, 7)$ or $(h, 0, 6.6)$, showing charge and spin order peaks at $\mathbf{Q}_c = (2n \pm \epsilon_c, 0, l)$ and $\mathbf{Q}_s = (2n \pm \delta_s, 0, l)$, respectively. Solid lines are Lorentzian fits; broken lines trace $\epsilon_c \sim 2\delta_s$. Peak at (007) contains superlattice Bragg intensity resulting from the LTO distortion but is contaminated by lattice Bragg scattering of $\lambda/2$ neutrons. (b) sketch of glassy charge-ordered state with a mixture of different commensurate superlattice fragments accommodating the nominal doping $x \approx 0.7$; (c) antiferromagnetic correlations governed by $\text{Co}^{2+}-\text{Co}^{3+}-\dots-\text{Co}^{2+}$ superexchange between Co^{2+} spins (arrows) developing in this CO state.

4 (b). Weiss temperature Θ_W and Co effective magnetic moment resulting from the Curie-Weiss analysis of its T -dependence are shown in Figure 1(d) and (c).

For neutron diffraction studies we used $\approx 20 \text{ mm}$ long, $\phi \approx 6 \text{ mm}$ cylindrical single crystal pieces of $m \approx 2 \text{ g}$. Mosaic of the fundamental Bragg reflections was $\lesssim 0.5^\circ$, which is consistent with the instrumental resolution and shows high crystalline quality. Neutron experiments were performed on 4G and 5G 3-axis thermal neutron spectrometers at the JRR-3 at JAEA, Tokai, Japan, with $40' - 40' - 40' - 40'$ beam collimation and BT9 spectrometer at the NIST Center for Neutron Research, with beam collimation $\approx 40' - 47' - 44' - 80'$ (open). Wave vector of the incident and scattered neutrons was selected by the (002) Bragg reflection from pyrolytic graphite (PG) and fixed at $k_i \simeq 2.67\text{ \AA}^{-1}$. Contamination from higher order reflections was suppressed by $1'' - 2''$ thick PG transmission filters. Sample was mounted in a closed-cycle He gas refrigerator ($T \geq 0.7 \text{ K}$) with $a - b$ plane vertical and $(h0l)$ reciprocal lattice zone in the horizontal scattering plane. We index wave vectors in the F4/mmm lattice with the unit cell $\sqrt{2}a \times \sqrt{2}a \times c$ compared to the I4/mmm high-temperature tetragonal (HTT) lattice of cuprates with $a \approx 3.8\text{ \AA}$. We assign "LTO" index to the in-plane lattice parameters thus defined, Figure 1(b), since our samples are actually in the low-temperature orthorhombic (LTO) phase, but the orthorhombic distortion is way too small to be resolved in the present measurements [22].

Typical low-temperature scans along h_{LTO} direction, revealing superlattice scattering in several PCCoO samples are shown in Figure 2. Two sets of peaks whose posi-

tion varies roughly linearly with doping can be identified. Sharper and more intense peaks at $\mathbf{Q}_s = \mathbf{G} \pm (\delta_s, 0, l)$, where \mathbf{G} is the wave vector of a fundamental lattice Bragg reflection, quickly disappear upon heating to $T \gtrsim 40$ K and decrease in intensity with increasing Q_s for different \mathbf{G} , roughly following the square of the Co^{2+} magnetic form factor. Hence, we identify these peaks as magnetic scattering arising from spin order. Their position varies roughly linearly with the remaining Co^{2+} content, $\delta_s(x) \sim (1-x)$. Weak diffuse peaks at $\mathbf{Q}_c = \mathbf{G} \pm (\epsilon_c, 0, l)$, whose position varies roughly as $\epsilon_c(x) \sim 2(1-x)$, are much broader and in fact increase in intensity with increasing Q_c in different \mathbf{G} zones, roughly $\sim Q_c^2$. We therefore identify them as superstructural scattering arising from atomic displacements accompanying short-range charge/valence order. These peaks remain unchanged both in width and intensity upon heating to $T \approx 300$ K.

Strong peak at $(1, 0, 7)$ is consistent with Bragg scattering arising from the LTO lattice distortion. Its intensity grows rather gradually below ≈ 300 K and then usually decreases below $T \sim 100$ K. Similar peak is present at other integer l , in particular at $l = 6$. This type of reflections was observed by neutron diffraction in the undoped La_2CoO_4 [17]. As $x \rightarrow 0.5$, $\epsilon_c(x) \rightarrow 1$ and LTO Bragg scattering at $h = 1$ overlaps with weak CO peak at $\mathbf{G} \pm \mathbf{Q}_c$. The latter, however, persists to much higher temperature, $T \sim 700 - 800$ K, and is much broader. The lower scan in Fig. 2(a) for $x = 0.56$ performed at $l = 6.6$ has only weak Bragg contribution at $h = 1$, while CO scattering is practically unchanged compared to $l = 7$.

The l -dependence of CO scattering measured in our PCCoO samples shows no peaks due to inter-plane coherence ($\xi_c^l \lesssim 0.2c$), but smooth intensity modulation resembling that reported for $x = 0.5$ LSCoO [18]. This indicates that scattering arises from similar distortions of CoO_6 octahedra, which are associated with charge polarons. In $x = 0.46$ and 0.39 PCCoO samples CO peak is at $h = 1$, indicating a finite region of stability of the CCO at $x \leq 0.5$. The in-plane peak width in these samples is comparable to that in $x = 0.5$ LSCoO, corresponding to CCO correlation length ξ_c^h of 3–5 LTO lattice spacings. For $x \geq 0.5$, where polaron correlations are incommensurate, CO peaks are at least twice broader, corresponding to $\xi_c^h \lesssim 10\text{\AA}$. Despite different tolerance factors and band-widths compared to PCCoO, our $x = 0.61$ LSCoO sample shows very similar glassy CO and SO correlations, which follow the same doping trend.

The picture of CO at $x \geq 0.5$ arising from these observations is illustrated in Figure 2(b). Polarons associated with Co^{2+} sites, whose concentration is $n_e = 1-x$, build up patches of commensurate superlattices corresponding to $n_e = 1/2, 1/3, 1/4, \text{etc.}$, where particular n_e is locally favored by La/Sr doping fluctuation. Their long-range coherence, however, is frustrated by the charge neutrality condition imposed by the average Sr^{2+} concentration x . Hence, glassy CO state results, which is made of a

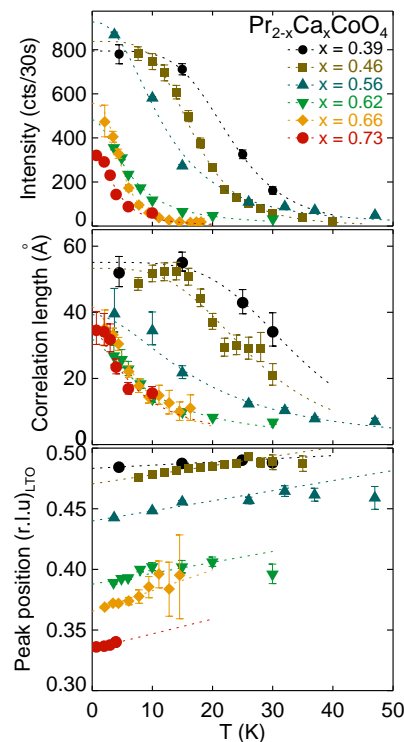


FIG. 3: Temperature dependence of magnetic SO peak parameters in PCCoO. (a) peak intensity cross-normalized to ≈ 30 sec BT9 monitor count for equal sample mass; (b) in-plane correlation length ξ_{ab} (inverse half-width at half maximum (HWHM) of Lorentzian fit); (c) peak position.

mixture of ~ 1 nm sized domains of commensurate polaron superlattices, accommodating the average charge doping. Consequently, CO scattering has an average incommensurability of $\epsilon_c(x) \approx 2(1-x)$.

Magnetic SO scattering with roughly half the CO incommensurability simply corresponds to the antiferromagnetic order of Co^{2+} spins, Figure 2(c). Magnetic correlations are apparently governed by $\text{Co}^{2+} - \text{Co}^{3+} - \dots - \text{Co}^{2+}$ superexchange (note that $\Theta_W > 0$ for all x , Fig. 1(d)). They decrease with increasing number of intervening Co^{3+} , but also extend between the different CO superlattice domains, which explains why the in-plane SO correlation length ξ_s^h is 3-4 times larger than ξ_c^h . This also explains the decrease with x of the SO temperature seen in panel (a) of Figure 3, which shows the T-dependence of the SO peak parameters. Typical of a glassy spin freezing, SO peak intensity increases smoothly with decreasing T, while the correlation length ξ_s^h , Figure 3(b), increases and seems to saturate roughly where the intensity reaches half its maximum. The temperature dependence of the SO peak position, Figure 3(c), also shows an interesting trend, which can be simply understood in this model. Indeed, as longer-periodic CO polaron superlattices present in a given sample gradually develop spin correlations with decreasing T, the average magnetic modulation period becomes longer and $\delta_s(T)$ decreases. Similar to the CCO case in $x = 0.5$ LSCoO,

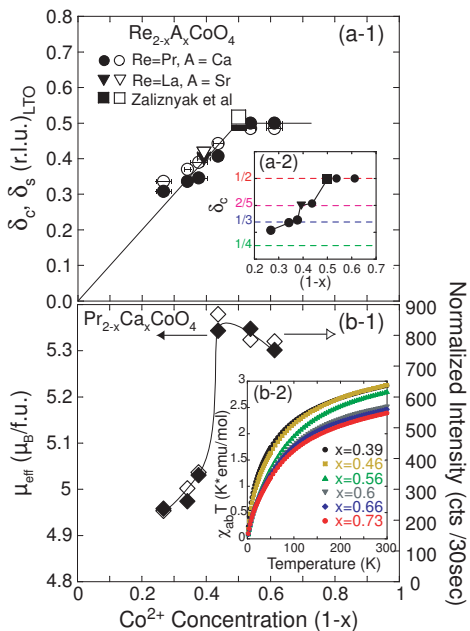


FIG. 4: (a) Diagram of the propagation vector for spin and charge superstructures in PCCoO and LSCoO. Filled (open) symbols show the in-plane modulation vector for charge (spin) order, $\delta_c = \epsilon_c/2$ and δ_s , respectively. Inset (a-2) is the enlarged Yamada plot showing the lattice commensurability effect on the position of CO peaks at $(2\delta_c, 0, l)$. (b) Concentration dependence of μ_{eff} (filled symbols) and peak magnetic neutron scattering intensity (open) in PCCoO. Inset (b-2) shows the temperature dependencies of $T \cdot \chi_{ab}$ for selected x 's. Lines are guides for the eye.

CO is totally uncoupled from SO, which simply follows the CO pattern.

The doping dependencies of the incommensurabilities of charge and spin order are summarized in Figure 4(a). As mentioned before, for $x \geq 0.5$ both roughly follow the $\sim 1 - x$ trend, although $\delta_s(x)$ is always somewhat larger than $\delta_c(x)$, corresponding to shorter average SO modulation period. This again is consistent with the picture where shorter-periodic polaron superlattices have better developed spin correlations. Detailed investigation of the CO peak position, Fig. 4(a-2), shows lattice commensurability effect on CO, indicating that most observed CO peaks can be assigned to a mixture of two nearest commensurate superlattices [6, 7].

Finally, we comment on an apparent doping-induced Co spin state change, which is manifested by a decrease of $\mu_{\text{eff}}(x)$ and in PCCoO occurs at $x \gtrsim 0.56$, Figure 1(c). Comparison of Figure 4 (a) and (b) suggests that other than decrease of the SO peak magnitude coincident with that of μ_{eff} it does not have any significant effect on charge and spin ordering.

In summary, we have discovered doping-dependent charge and spin modulations in PCCoO and LSCoO, whose periods vary roughly linearly with doping, $\delta_s \sim \epsilon_c/2 \sim 1 - x$, existing for $x > 0.5$. They border the checkerboard CO phase at $x \lesssim 0.5$. In cobaltites CO

occurs in a phase where electrons are strongly localized and can therefore be understood as a correlated polaron glass with nanoscale patches of commensurate CO superlattices, whose long-range coherence is frustrated by the charge neutrality requirement. Antiferromagnetic SO correlations between the nearest "undoped" Co²⁺ sites develop at temperatures more than 100 times smaller than CO and do not affect it. Similar CO (but not SO) was found in layered manganites, where it also emerges from the state with thermally activated transport [23, 24]. There, though, polaron correlations are associated with the orbital order and double-exchange physics, which are absent here. CO and SO in cobaltites are most likely governed by the lattice electrostatics and superexchange. However, in many respects they have quite similar appearance to CO/SO in cuprates and nickelates, showing ubiquity of this type of pattern.

We thank T. J. Sato and K. Hirota for help with experiments. This work was partly supported by Grant-In-Aids for Scientific Research (C) (No. 16540307) from the Ministry of Education, Culture, Sports, Science, and Technology, Japan, and by the US DOE under the Contract DE-AC02-98CH10886.

* Address correspondence to zaliznyak@bnl.gov

- [1] J. M. Tranquada, *et al.*, Nature **375**, 561 (1995).
- [2] M. Fujita *et al.*, Phys. Rev. B. **65**, 064505 (2002).
- [3] S. A. Kivelson, *et al.*, Rev. Mod. Phys. **75**, 1201 (2003).
- [4] C. H. Chen, *et al.*, Phys. Rev. Lett. **71**, 2461 (1993).
- [5] J. M. Tranquada, *et al.*, Phys. Rev. B **52**, 3581 (1995).
- [6] H. Yoshizawa, *et al.*, Phys. Rev. B **61**, R854 (2000).
- [7] R. Kajimoto, *et al.*, Phys. Rev. B **67**, 014511 (2003).
- [8] S.-H. Lee, *et al.*, Phys. Rev. Lett. **88**, 126401 (2002).
- [9] J. Zaanen, O. Gunnarsson, Phys. Rev. B **40**, 7391 (1989).
- [10] V. J. Emery, S. A. Kivelson, Physica C **209**, 597 (1993).
- [11] L. Pryadko, *et al.*, Phys. Rev. B **60**, 7541 (1999).
- [12] M. Ichioika, K. Machida, J. Phys. Soc. Jpn. **68**, 4020 (1999).
- [13] N. Ichikawa, *et al.*, Phys. Rev. Lett. **85**, 1738 (2000).
- [14] V. I. Anisimov, *et al.*, Phys. Rev. Lett. **68**, 345 (1992).
- [15] J. Zaanen, P. B. Littlewood, Phys. Rev. B **50**, 7222 (1994).
- [16] D. I. Khomskii, K. I. Kugel, Phys. Rev. B **67**, 134401 (2003); Europhys. Lett., **55**, 208 (2001).
- [17] K. Yamada, *et al.*, Phys. Rev. B **39**, 2336 (1989).
- [18] I. A. Zaliznyak, *et al.*, Phys. Rev. Lett. **85**, 4353 (2000); Phys. Rev. B **64**, 195117 (2001).
- [19] Magnetic susceptibility data of Ref. 20 indicate change to a lower-spin Co³⁺ state with doping at $x \sim 0.7$.
- [20] Y. Moritomo, *et al.*, Phys. Rev. B **55**, R14725 (1997).
- [21] T. Matsuura, *et al.*, J. Phys. Chem. Solids **49**, 1403 (1988).
- [22] A. T. Savici, *et al.*, Phys. Rev. B. **75**, 184443 (2007).
- [23] W. Bao, *et al.*, Sol. Stat. Comm. **98**, 55 (1996).
- [24] S. Larochelle, *et al.*, Phys. Rev. B **71**, 024435 (2005).